Calibration sources and filters of the soft x-ray spectrometer instrument on the Hitomi spacecraft

Cor P. de Vries
Daniel Haas
Noriko Y. Yamasaki
Jan-Willem den Herder
Stephane Paltani
Caroline Kilbourne
Masahiro Tsujimoto
Megan E. Eckart
Maurice A. Leutenegger
Elisa Costantini
Johannes P. C. Dercksen
Luc Dubbeldam
Martin Frericks
Phillip P. Laubert
Sander van Loon
Paul Lowes
Alec J. McCalden
Frederick S. Porter
Jos Ruijter
Rob Wolfs

SPIE.

Calibration sources and filters of the soft x-ray spectrometer instrument on the Hitomi spacecraft

Cor P. de Vries,[a,*] Daniel Haas,[a,b] Noriko Y. Yamasaki,[c] Jan-Willem den Herder,[a] Stephane Paltani,[d] Caroline Kilbourne,[e] Masahiro Tsujimoto,[c] Megan E. Eckart,[e] Maurice A. Leutenegger,[e] Elisa Costantini,[a] Johannes P. C. Dercksen,[a] Luc Dubbeldam,[a] Martin Frericks,[a] Phillip P. Laubert,[a] Sander van Loon,[a] Paul Lowes,[a] Alec J. McCalden,[a] Frederick S. Porter,[e] Jos Ruijter,[a] and Rob Wolfs[a]

[a]SRON Netherlands Institute for Space Research, Utrecht, The Netherlands
[b]Airbus Defence and Space, Friedrichshafen, Germany
[c]Institute of Space and Astronautical Science, Japan Aerospace Exploration Agency, Sagamihara, Kanagawa, Japan
[d]University of Geneva, Department of Astronomy, Versoix, Switzerland
[e]NASA/Goddard Space Flight Center, Greenbelt, Maryland, United States

Abstract. The soft x-ray spectrometer was designed to operate onboard the Japanese Hitomi (ASTRO-H) satellite. In the beam of this instrument, there was a filter wheel containing x-ray filters and active calibration sources. This paper describes this filter wheel. We show the purpose of the filters and the preflight calibrations performed. In addition, we present the calibration source design and measured performance. Finally, we conclude with prospects for future missions. © *The Authors. Published by SPIE under a Creative Commons Attribution 3.0 Unported License. Distribution or reproduction of this work in whole or in part requires full attribution of the original publication, including its DOI.* [DOI: 10.1117/1.JATIS.4.1.011204]

1 Introduction

The soft x-ray spectrometer (SXS)[1] was the x-ray microcalorimeter spectrometer onboard the Hitomi (ASTRO-H) mission.[2] This satellite was launched on 17 February, 2016, but unfortunately, during the initial commissioning observations,[3] the mission suffered a premature end on 26 March, 2016.

The SXS detector array[4] is a 6×6 array of square pixels arranged with a 0.832-mm pitch, kept at a temperature of 50 mK, mounted inside a Dewar. The detector array has a minimum energy range of 0.3 to 12 keV and demonstrated an inflight energy resolution of 4.9 eV.[5] In the beam, inside the Dewar, a fixed stack of thin filters is mounted,[6] with each filter at a different temperature corresponding to the different Dewar shells. The purpose is to suppress incident optical and infrared radiation on the microcalorimeter pixels, minimizing background levels.

Although the detector operating temperature is maintained by means of active control of the adiabatic demagnetization refrigerator (ADR) coolers,[7] the gains or energy response of the pixels is expected to change, both with respect to the calibration and with respect to each other. The two main sources of drift are changes in the conductive thermal loading of the control thermometer and changes in the radiative loading of the calorimeter pixels as a result of changes in the warmer temperature stages of the Dewar. After the Dewar temperatures reached a steady state in orbit, these temperatures continued to be perturbed by the heat of magnetization dumped from recycling the ADR. Increased loading of the thermometer as a result of warming in the Dewar resulted in control of the ADR at a lower temperature and an associated increase in gain.

Increased thermal radiation on the pixels as a result of warming in the Dewar resulted in a reduction in gain that depended on the location of the pixel. These effects tended to cancel but not nearly well enough, thus gain monitoring was imperative. The prime monitoring aid was a small radioactive ^{55}Fe source that illuminated one separate detector pixel, mounted in a corner, outside of the actual detector array. Monitoring the stability of the main ^{55}Mn 5.889-keV radioactive decay x-ray line emission allows primary calibration of the detector array. However, differences over the detector array cannot be traced in this way. This required a separate calibration source.

At a distance of about 90 cm from the detector plane, well outside the Dewar, a filter wheel (Fig. 1) is mounted on the spacecraft structure. This wheel contains six positions (Fig. 2), and it is able to rotate a suitable filter into the beam, in order to optimize the quality of the data depending on the characteristics of the astrophysical source. It was chosen to have two open positions on opposite locations in the filter wheel, two x-ray filters: namely, a beryllium filter and a neutral density filter, and a filter (polyimide) largely transparent to x-rays but able to block possible contamination from the telescope. Finally, there is a filter-mount consisting of a ring of additional radioactive ^{55}Fe calibration sources that are able to homogeneously illuminate the detector.

On the filter-wheel mechanical structure, below the filter wheel in the direction toward the SXS Dewar, a set of electrically powered calibration sources is mounted. Each of these sources is able to illuminate the whole detector array, to enable absolute and relative gain calibration of all pixels in the array. The preflight development of the filters and calibration sources has been described previously in Refs. 8 and 9.

During the short in-flight operational lifetime of the satellite, a closed-gate valve in the beam kept the vacuum in the Dewar
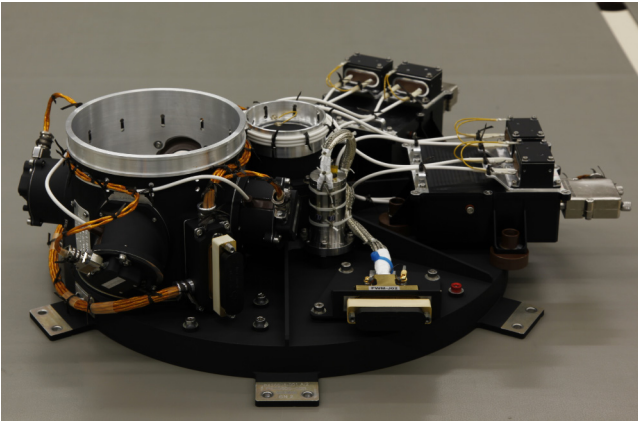
Fig. 1 Photograph of the complete filter wheel assembly from the top. The top ring is directed toward the SXS Dewar. Figure 3 shows the different parts. Total mass is about 4.5 kg. (Clarification of the different parts is given in Fig. 3).
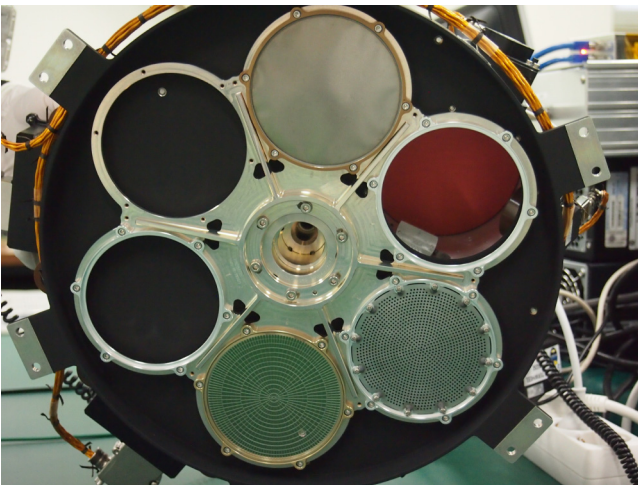

Fig. 2 Photograph of the bottom of the filter wheel assembly showing the actual filters rotating disk. The hole of the telescope beam is on the upper right, where an orange (temporary) protection cap is visible. Individual filter holders have a diameter of about 10 cm; the total wheel has a maximum diameter of 32 cm. (Filter identifications are given in Fig. 4).
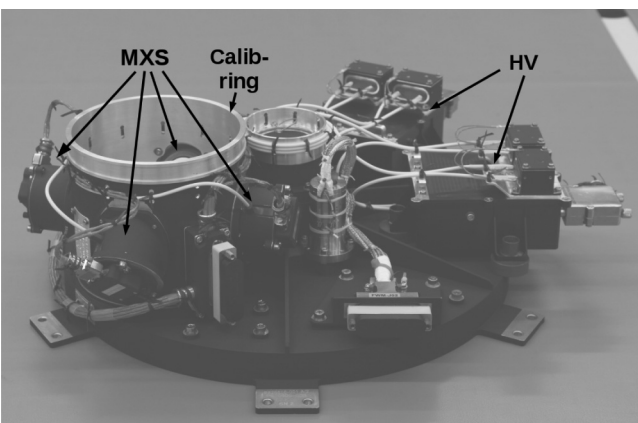

Fig. 3 Clarification of the different parts of the filter wheel. The HV power supplies for the MXSs are located on the right. The cylinder on the left, the "calibration ring" (calib-ring), is the beam opening containing the MXSs (MXS). Diameter of the assembly is around 38 cm.
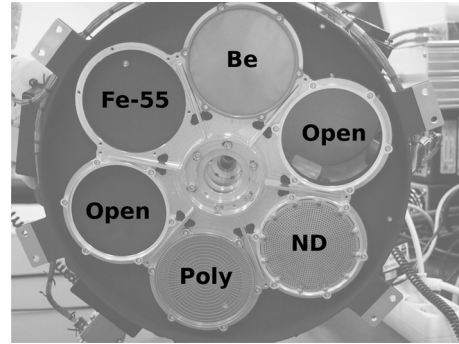

Fig. 4 Positions of the different filters in the filter wheel. Compare with Fig. 2. "Open" are the two open positions. "Be" is the position of the beryllium filter. "ND" is the neutral density filter and "Poly" is the polyimide anticontamination filter. "Fe-55" marks the position of the ^{55}Fe radioactive sources, which, however, on the photograph is not yet mounted.

free from the initial out-gassing of the satellite. This gate valve contained ∼262-μm-thick beryllium window with a support structure.[10] This window blocked low-energy x-rays.

The scope of this paper is to provide a reference on the Hitomi SXS filter wheel, which is useful for understanding the gain calibrations performed on the actual observations done with the satellite. In addition, a description of the hardware, calibrations, and tests, as well as the arguments for the specific choices that were made, can be very useful for future missions that are considering to fly comparable hardware.

2 Active MXS Calibration Sources

Below the actual filter wheel, on the calibration ring (see Fig. 1), a set of four modulated x-ray sources (MXS) is mounted. Two sources illuminate the SXS detector directly and two sources illuminate the SXS via a fluorescent target to generate lines of low x-ray energy (see Fig. 5).

2.1 MXS Design

An early concept of generating x-rays by means of electrons generated by the photoelectric effect was proposed by
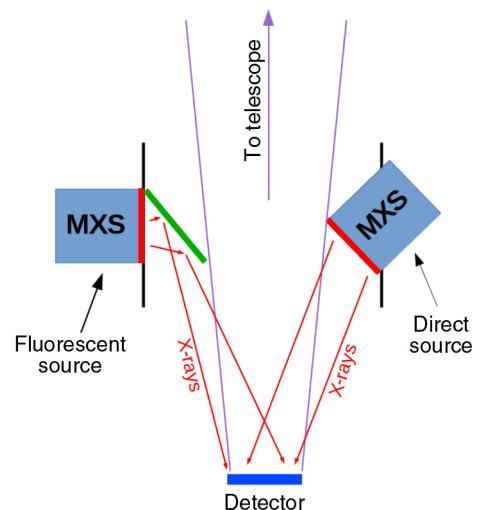

Fig. 5 Schematics of the MXS layout in the telescope beam (not to scale).
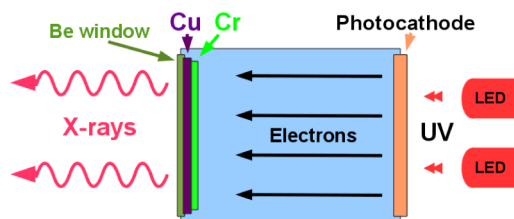
Fig. 6 Schematic principle of an MXS.

Gendreau[11] (More information can be found from a later document at Ref. [12]). Our design of the MXSs is based on a modified image intensifier unit (made by Photonis). It is a short vacuum tube with a photocathode on one end and a beryllium vacuum window on the other end. Light from two light-emitting diodes (LEDs) illuminates the photocathode, producing electrons, which in turn are accelerated by a 11.3-kV high voltage (HV) toward a target material sitting on top of a 300-μm beryllium window. Generated x-rays exit the source through the target and the beryllium window (see Fig. 6).

X-rays will only be produced when the LED is emitting light. This allows for short duration x-ray pulses. In this way, continuous monitoring of the performance of each detector during astronomical observations is possible by selecting only those short-time periods in which the LED is on, leaving, in the remaining time, the observed astrophysical spectrum uncontaminated by the broadband spectrum emitted by the MXS.

Although the photocathode material (S20) has maximum quantum efficiency (QE) at wavelengths below 280 nm, maximum yield in terms of number of electrons, which is proportional to the number of generated x-ray photons, is at 420-nm wavelength (see Fig. 7). For a typical value of 5 mW of optical energy, this means an output of 2×10^{15} electrons/s. In the final

Fig. 8 Spectrum of the MXS obtained with low-resolution SDD. On top of the Bremsstrahlung continuum, the lines of Cr and Cu can be seen. This spectrum was measured in air, which decreases the low-energy Cr lines somewhat.

flight version of the MXS, blue LEDs were used with maximum output power at 460 nm.

The target consists of a layer of 25 nm of chromium on top of 150 nm of copper deposited on the beryllium window. These two types of material will generate two sets of x-ray lines: the Cu K_α and K_β lines at 8.05 and 8.90 keV, respectively, and the Cr K_α and K_β lines at 5.41 and 5.95 keV, respectively. The electrons will hit the chromium first. Although this order of layers will have lower efficiency generating the Cu lines, it does offer the possibility of generating the Cr lines only, when the HV is operated at a lower voltage than the nominal voltage of 11.3 kV. Figure 8 shows a measured spectrum [measured with a low-resolution silicon drift detector (SDD)], showing the chromium and copper lines plus the Bremsstrahlung continuum. For comparison, Fig. 9 shows the high-resolution spectrum measured with the SXS during the thermal vacuum test of the satellite. Due to the thick beryllium window on the Dewar gate valve, the chromium lines measured during the thermal vacuum tests are suppressed compared to what we expect for normal operations on-orbit (after the gate valve was opened).
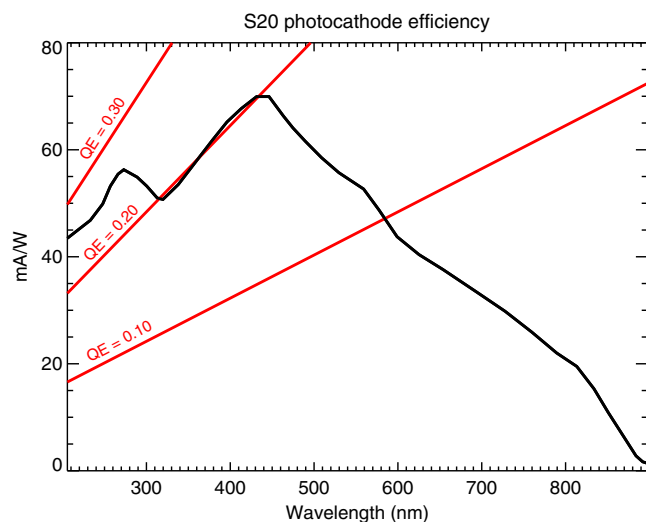

Fig. 7 S20 photocathode efficiency (provided by the Photonis Company). Black line shows the photocurrent (mA) related to optical power (W) as function of wavelength. The red lines show an overlay of coordinates of constant QE which represent the ratio in which electrons are generated as function of the number of incoming optical photons. Maximum QE (around 26%) is around 270 nm, but maximum cathode efficiency is at 440 nm, where QE is only 20%. This is due to the larger number of photons at longer wavelength for the same optical power.
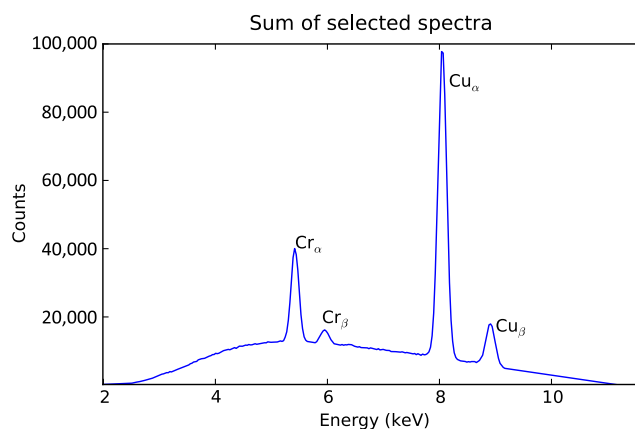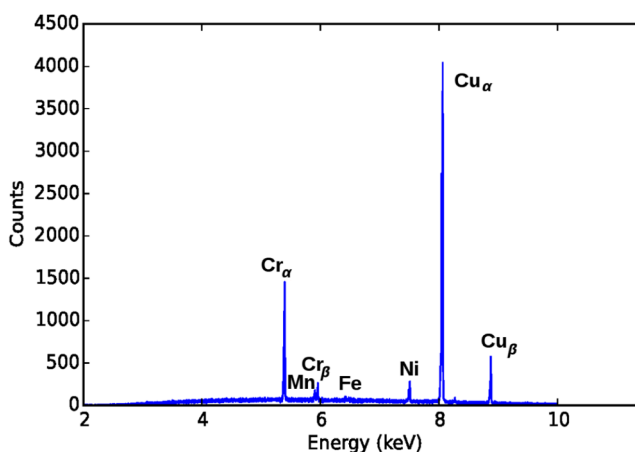

Fig. 9 Similar to Fig. 8, but now measured with the high-resolution SXS during a satellite TV test. Apart from the Cu and Cr lines, fluorescent lines of a few other elements (Ni 7.478 keV, Fe 6.403 keV) present on the MXS housing can be seen. In addition, a weak ^{55}Mn 5.895-keV line from the radioactive source on the filter wheel is visible.

Fig. 10 A bare MXS source, without source holder and LEDs, showing the size, next to a 1€ coin, for comparison. The top of the source shows the beryllium exit window.

In addition, the blocking geometry of the gate valve window support structure enhances the additional Fe and Ni fluorescent lines from the MXS housing.

Two types of MXS sources exist. Each type is present as a redundant pair, which gives a total of four sources. One type is the so-called direct source type, which illuminates the SXS with the x-ray spectrum generated by the Cr/Cu anode as shown in Fig. 6. These sources are mounted with a 45-deg angle (see Fig. 5) with respect to the telescope optical axis, in order to move the MXS exit window as close to the telescope beam as possible. The other type is an indirect source, which has low-energy fluorescent targets mounted in front of the MXS exit window. These fluorescent targets allow the low-energy lines of aluminum (1.49 keV) and magnesium (1.25 keV) to be incident on the SXS. The MXS vacuum windows absorb these low-energy photons, hence they must be generated (in vacuum) outside of the MXS. Due to the low fluorescent yield, the "indirect" source strength will be much lower than the "direct" sources. For the same settings (LED current and
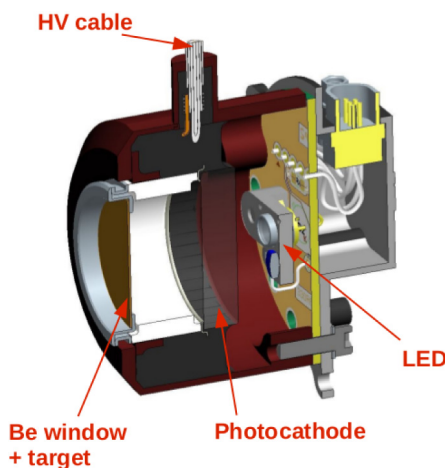

Fig. 11 Drawing of a crosscut through the MXS source mounted in its holder (diameter 5.1 cm, length 3.1 cm), showing the LEDs on the right, illuminating the photocathode. The beryllium window, which contains the x-ray target, is to the left.
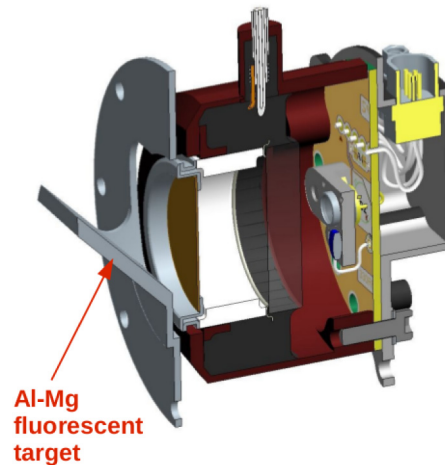

Fig. 12 Drawing of a crosscut through the fluorescent MXS source, with the Al-Mg fluorescent target mounted in front of the MXS.

duty cycle), the fluorescent sources are estimated to be about a factor in between 100× to 1000× weaker than the direct sources. For this reason, these fluorescent sources will not be pulsed, such as the direct sources, but operated (occasionally) in a continuous mode. This multitude of available calibration lines from the low (fluorescent) to the higher (direct source) energies allows calibration of nonlinearities in the SXS pixel response. Information on the detailed shapes of the lines present in the MXS spectrum can be found elsewhere.[13]

Figure 10 provides an idea of the actual size of an MXS source. Figures 11 and 12 show a crosscut of the actual direct and fluorescent sources design.

2.2 MXS Performance

In order to monitor the (slowly) varying SXS pixel gains during observations, it was estimated that a flux of 0.3 counts/s/SXS pixel from the MXS calibration lines would be required. This flux translates into 5×10^6 photons/s at the MXS source, given a source–detector distance of about 85 cm and pixel size of 0.82 mm. The 0.3 counts/s estimate was based on a required energy scale stability of around 0.5 eV and the assumption that typical time scales of SXS gain variation would be in the order of 10 min. Terms in the detector noise budget were based on tracking gain changes in 10-min integrations, using the required limits on the temperature coefficients of the electronics. Also, given the orbital period of 90 min, the relevant tracking time scale was around 10 min. Based on ground operations, temperature changes within the Dewar were expected to be much slower than the 10-min time scale and, thus, could be well tracked in 10-min integrations.

The sources are expected to show degradation over time, due to damage of the photocathode by ions generated by the electron impact on the target, and accelerated from the x-ray target back to the photocathode. Hence, source degradation with time is a function of the generated x-ray flux.

The direct sources are intended to be operated in a pulsed mode. The source intensity can be varied by changing the LED current. In addition, the time-averaged flux depends on the duty cycle of the LED pulses.

Several lifetime tests were performed to demonstrate that the MXS flux requirements could be met during the design life of the satellite mission with nominal operations of the MXS

sources. In a first test,[9] a source was initially set to operate at 100× the required flight values. This was accomplished by running the source at a 100% duty cycle (continuous operations). LED current was kept constant and the flux was allowed to decrease during the tested time period. With this setup, the source is expected to degrade a factor of 100 faster than during the nominal flight operations, which use 1% duty cycle. This was confirmed when comparing the observed degradation at the 100% duty factor with a long measurement at nominal (1% duty cycle) operations. The degradation at 1% was 100 times slower than at 100% duty cycle.

It was found that the flux half-life of a direct source during such operations will be 2.9 years. Renormalizing the flux at the end of the test to the initial flux levels by increasing LED current, it was found that given the observed half-life of the source, the required LED current at the nominal end of mission (5 years) would be well below the maximum allowed LED current of 40 mA.

A second lifetime test was conducted, controlling the MXS to operate at a constant flux level. The source was operated at 50% duty cycle at a time-averaged flux, which was 50× the nominal flux required in flight. The MXS flux during the LED pulse was identical to the intended flux in flight during pulses, but pulse duration during the test was 50× longer. This meant 1 week of the test was equivalent to about 1 year in orbit. The test was executed for a total of 1300 h, equivalent to about 7.4 years in orbit. Figure 13 shows the count rate during the test, together with the LED temperature. LED performance depends on temperature. The spiky character of the count rate curve is due to the periodic (automatic) updates of the LED current, to keep the count rate at an approximate constant level. (Each spike corresponds to steps of integer numbers in the DAC controlling the LED current. For this reason, the spikes decrease with time since the relative size of the integer steps decrease with increasing number, which corresponds to current). The count rate as shown in Fig. 13 is the one measured by the SDD detector in the test setup and corresponds to a source intensity providing 50× the 0.3 counts/s/pixel in the SXS. Figure 14 shows the
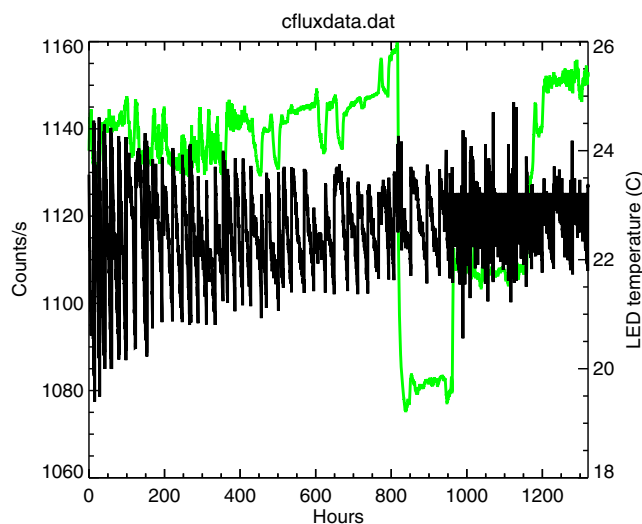

Fig. 14 LED current during the constant flux measurements. The sharp drop in room temperature (green line) also causes a drop in the LED current, due to the increased LED efficiency.

LED current during the test. The LED current increases due to the degradation of the source. At the very end of the test (equivalent of 7.4 years of the mission), the LED current is around 2.0 mA, well below the maximum allowed LED current of 40 mA. This test shows that the MXS can easily accommodate the nominal required flux during the 5 years of design mission lifetime. Figure 14 also shows the temperature dependence of the LED performance. A drop in ambient temperature corresponds to a discontinuity in the LED current increase.

In addition, the relation between source degradation and peak flux during LED pulses was investigated. The time-averaged flux is the result of the pulse duty cycle and the flux within the pulse. A lower duty cycle can give the same time-averaged flux when the LED current is higher. Figure 15 shows the increase in LED current when the flux is kept constant, but the duty cycle is changed. For the low duty cycle (high LED

Fig. 13 Count rate plot during the test. The green line is the LED temperature, corresponding to the room temperature during the test. The room temperature was changed on purpose (the sharp drop to 20 C) to see the effect of a temperature change.
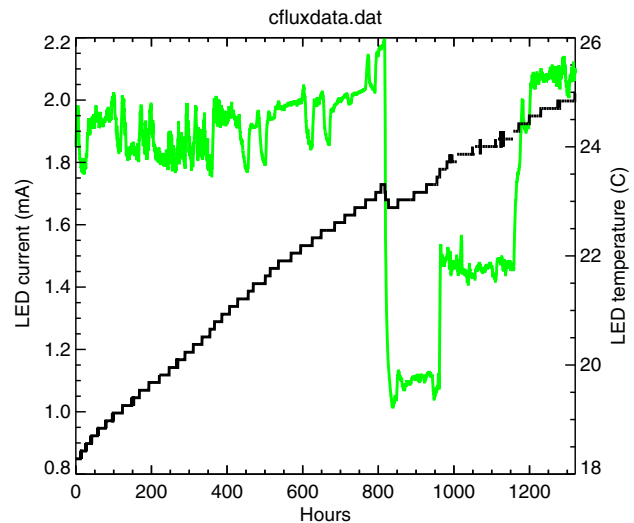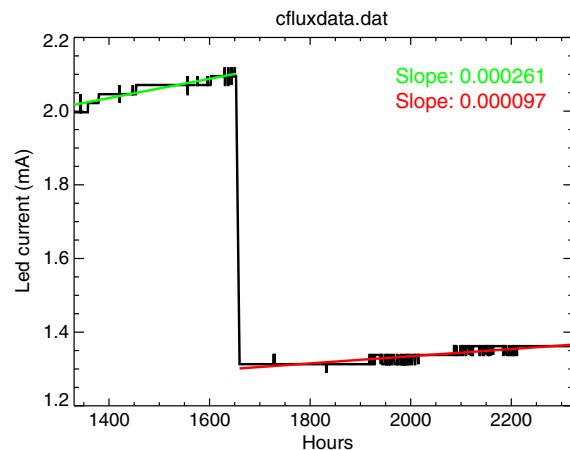

Fig. 15 Linear fits to the LED current increase due to aging of the MXS around the time when the LED current in the pulse is dropped by a factor of two (around the time stamp of 1650 h in the test) and duty cycle is doubled. The average x-ray flux remains the same in this way. It shows that at half the LED current (and double duty cycle), aging goes less than twice slower for the same x-ray flux.
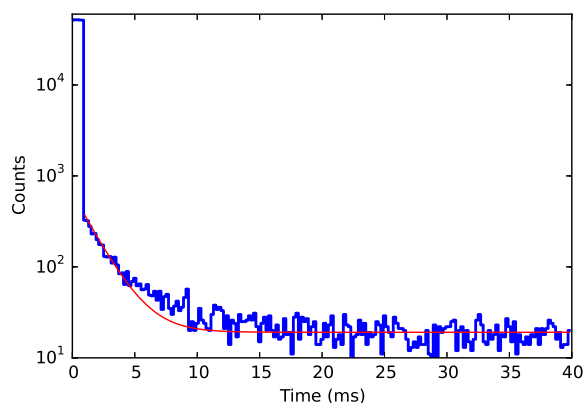
Fig. 16 MXS pulse shape (logarithmic scale) for a 1-ms pulse within a 40-ms pulse cycle, using nonflight electronics. The "pulse tail" starts at 0.7% of the original pulse flux, exponentially decaying to a background level (not associated with the MXS). The red line is the fitted exponential curve with 1.7-ms e-folding time.

Fig. 17 MXS pulse shape (logarithmic scale) for a 5-ms pulse, from the Hitomi thermal-vacuum tests, using the flight electronics. As can be seen, the decay of the pulse tail is much slower and the tail starts at higher levels, compared to the MXS using nonflight electronics (Fig. 16).

pulse current), the increase is 261 ± 30 nA/h, whereas for the high duty cycle (low LED pulse current), the increase is 97 ± 4 nA/h. It appears that the increase in the current (and thus the degradation of the source) is lower when the flux at the pulse (proportional to the LED pulse current) is lower. Hence, the source will degrade faster when the flux during the pulse is set to higher levels, even if the time-averaged flux remains constant.

Finally, the MXS response over time was investigated. This was done using nonflight electronics in a special setup. Figure 16 shows the MXS flux as function of time within the MXS pulse cycle. A 1-ms LED pulse was executed within a 40-ms cycle time. As can be seen, the original flux in the pulse of 5.2×10^4 events/bin drops within one-time resolution bin (0.2 ms) to about 400 events/bin (0.7% of the initial flux) and then exponentially decreases to the background level with an e-folding time of 1.7 ms. Although the photocathode material (S20) is supposed to react very fast, at μs time scales, to changing light levels (the same material is also used in photomultiplier tubes), it may be that positive ions released by the impact of electrons on the anode continue to (re)activate the cathode or that the abundant x-ray photons interact with the cathode, slowing down the expected fast response.

The above measured x-ray response is the response of the MXS itself. Unfortunately, the flight electronics generating the LED pulse for the filter wheel had an e-folding time of about 5 ms. Thus, the MXS pulse on the filter wheel had a slower decay than an isolated MXS by itself (see Fig. 17).

2.3 MXS High-Voltage Control

Each (main/redundant) MXS pair of direct and fluorescent sources is powered by an HV unit. These units can be set to produce 500, 4000, 7000, or 11300 V. Primarily, these settings were designed to allow the voltage to be slowly ramped up to the default operating voltage of 11.3 kV. The lower 500-V setting was devised to be used during the satellite's South Atlantic Anomaly passages. The 7-kV setting was defined to allow the 5.41- and 5.95-keV Cr lines to become active only, without going to the highest voltage setting. Finally, the maximum voltage was, in part, limited by the operating boundaries specifications of the HV cables.
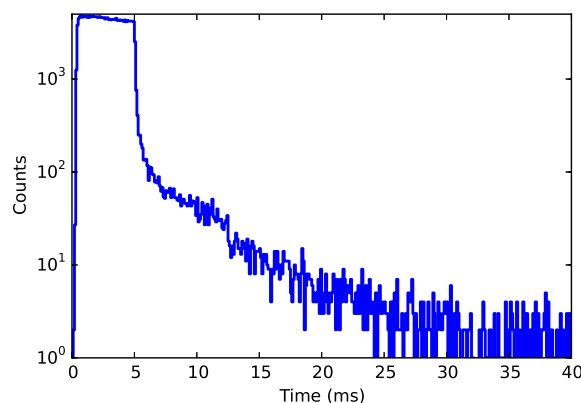
2.4 MXS-Intended Operations

The MXS calibration sources were planned to be switched on during the very contact pass when communications to the Hitomi satellite could not be established due to its problems. All operations stopped at that time. (The MXSs had only started on the 500-V HV setting when operations stopped.) Thus, no data on the actual flight performance were obtained.

For the MXS-intended operations, in order to minimize dead time, the duty cycle would be set to the lowest practical level, limited by the instantaneous flux that the MXS can safely produce during a pulse. The initial plan for normal flight operations was to start operating the direct sources at 1% duty cycle during most of the observing time, at a flux of 0.3 counts/s/pixel, depending on the SXS gain stability and background levels. In order to prevent energy-resolution degradation due to crosstalk in adjacent detector read-out channels, pulse width ideally should be set short enough that the expectation value for photon detection on three pixels in the same pulse is much less than one. Thus, in principle, optimization tends to be short periods but is limited by the time constant of the MXS response.

The fluorescent sources would be switched on occasionally, possibly once a day, to measure the nonlinear effects in the SXS response. Of course, an early learning period was foreseen in which the actual MXS operations would be tuned in order to allow for optimal dynamic calibration of the SXS.

3 Radioactive ^{55}Fe Calibration Sources

Figure 18 shows a picture of the ^{55}Fe sources ring, mounted in the filter wheel disk. The ring diameter is slightly larger than the beam at the position of the filter wheel. The cross structure coincides with the quadrant boundaries in the mirror when the mount is in proper position, centralized in the beam. At the four intersections of the cross with the ring and in the cross central position a total of five, ^{55}Fe sources are present. These sources allow a reasonably homogeneous illumination of all the SXS pixels when the calibration mount is rotated onto its nominal position in the beam.

Each ^{55}Fe source was designed to have a source strength of 6 MBq at the Hitomi launch time. During the radioactive decay (half-life 2.737 years) to ^{55}Mn, the source emits x-ray lines (^{55}Mn, K$_\alpha$, and K$_\beta$) at 5.895 and 6.490 keV.
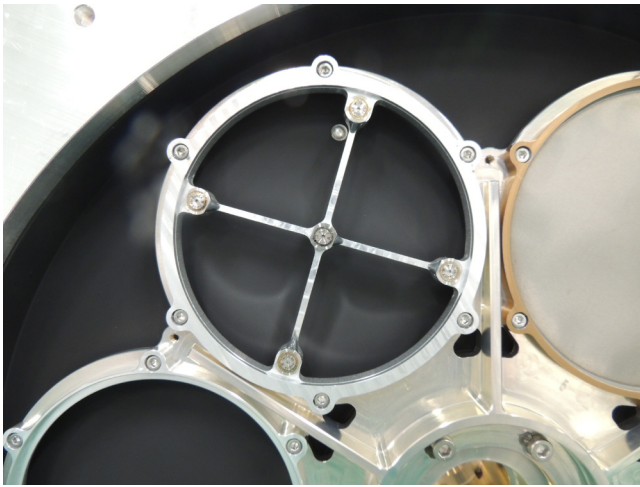
Fig. 18 Picture of the ^{55}Fe sources ring within the filter wheel disk, with the mounted radioactive sources. The sources are located on the end of the "cross" structure and in the center of the cross. Ring inner diameter is about 9 cm.

This ^{55}Fe calibration source was used early in flight to calibrate the relative gains of the SXS. Since the Dewar gate valve was still closed, the ^{55}Fe calibration mount was not put at its nominal position in the beam, but at a 10-deg angle, to allow the beams of the ^{55}Fe individual sources to bypass the gate valve window support structure. Otherwise, the window support structure would block most of the central part of the detector. Because of this 10-deg angle and some remaining shadows of the gate valve window structure, illumination of the SXS pixel array was not homogeneous. This was verified during the satellites thermal vacuum tests and in-flight operations. Figure 19 shows a ray trace plot of the SXS illumination by the rotated ^{55}Fe calibration mount.

4 X-Ray Filters

Two x-ray filters are present in the filter wheel. On a third position, initially, an optical filter was envisaged to block light from optically bright sources.[8] During the early phases of mission design, a set of thin Dewar filters was proposed, which would not block optical radiation for optically bright sources sufficiently. In the end, however, thicker Dewar filters were selected, superseding the need for a separate external optical filter. A polyimide-only filter (with stainless steel support) was kept in this place as a possible safeguard against contamination, to be used in case out-gassing of the top part of the satellite during early phases of the mission would exceed tolerable quantities.

The remaining x-ray filters consisted of a beryllium filter to block low-energy x-rays and a neutral density filter to decrease x-ray flux from bright objects (e.g., targets of opportunity). More details on the filter calibration can be found elsewhere.[10,14]

4.1 Beryllium Filter

A spectral region of great interest for the SXS spectrometer is around the Fe-K lines (6.4 keV and above). High count rates decrease the resolution of the instrument. At high count rates, a larger fraction of detected x-ray photons (events) end up as low-resolution grade events (see Fig. 20). Hence for bright sources, the energy resolution in the Fe-K region can be degraded by excess flux at low energies. To mitigate this effect,
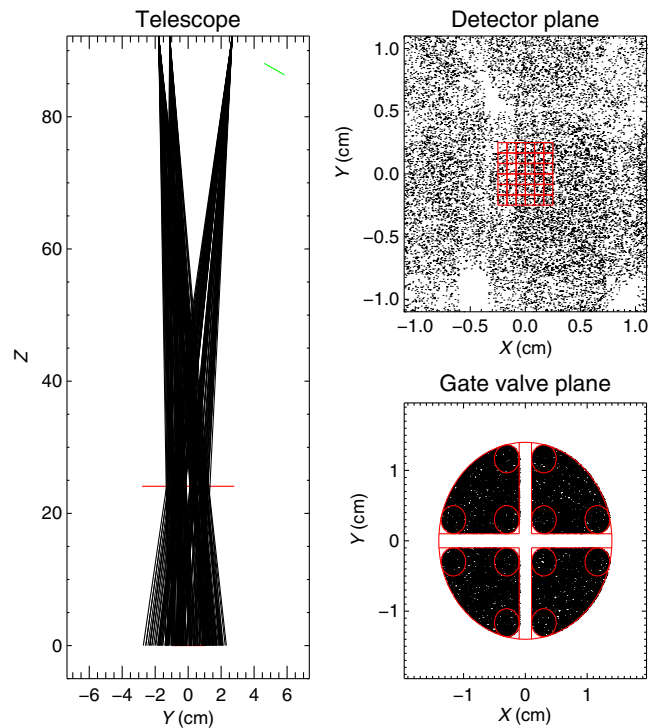

Fig. 19 Ray trace of the ^{55}Fe photons on the detector plane. The actual detector pixels are indicated. Due to the 10-deg rotation of the source mount, shadow patterns from the gate valve window structure can be seen.

the beryllium x-ray filter has been designed. Simulations were performed to estimate the effect of a beryllium filter on bright sources. It was found[8] that a typical black hole candidate transient (BHCT) type source represents the best case, in which a beryllium filter can improve the quality of the observations. Figure 21 shows the expected SXS effective areas when employing different Be filter thicknesses. Figure 22 shows the effect of the same filters on the number of observed high- and medium-resolution events for a BHCT model source. The number of good resolution events around the Fe-K band increase for all beryllium filter thicknesses. Although the most positive effect
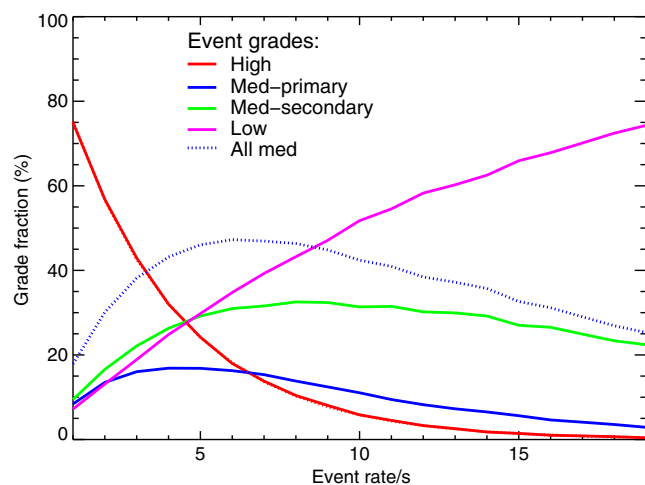

Fig. 20 Ratio of detected counts with respect to input photons for the different event grades[15] as function of flux. High grade events have the highest energy resolution.
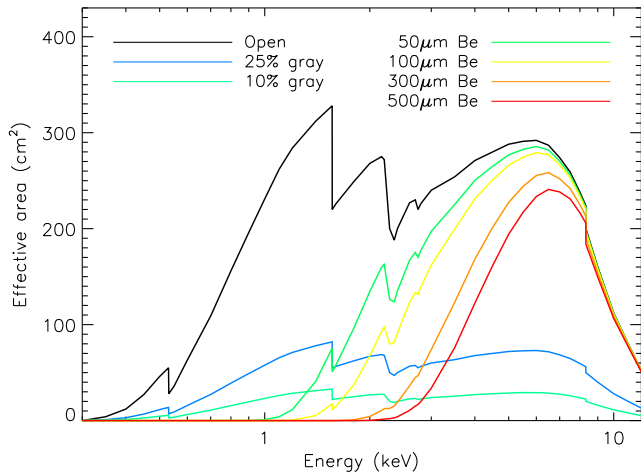
Fig. 21 SXS effective area for a (potential) set of different beryllium x-ray filters. In addition, the effect of 25% and 10% neutral density filters is shown.
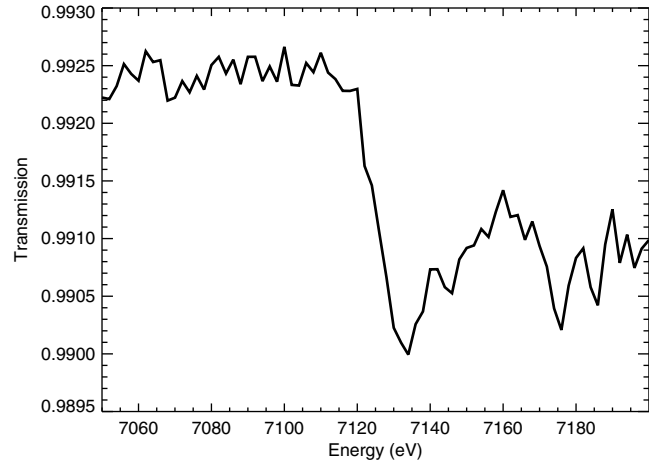

Fig. 23 Calibration of the transmission of a 25-μm beryllium filter around the Fe-K edge. A small drop of about 0.25% is observed. Measurement uncertainty is around a 0.0003 level in transmission.
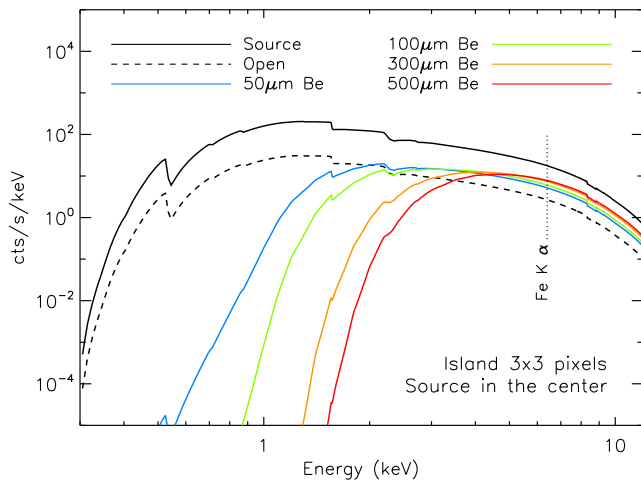

Fig. 22 Expected high- plus med-res (H+M) event counts for the beryllium filters applied to a model BHCT spectrum. The solid black line (labeled "source") are the expected number of events when all incident photons would be recorded as H+M events. Dashed line ("open") is the actual number of recorded (H+M) events when no filter is applied. Colored lines are the number of H+M events for the different beryllium filters.

is gained when employing the thickest filter, a filter with a beryllium thickness of 25 μm was selected for flight in order to preserve all types of science in case of a filter-wheel malfunction.

Two flight-model (FM) beryllium filters were calibrated at the Berlin Synchrotron (BESSY II) in terms of transmission. Unfortunately, due to a workmanship error, these filters were not able to withstand the launch vibration levels. Instead, a qualification model (QM) beryllium filter, for which it was proven that it could withstand the vibration levels, was mounted in the FM filter wheel. Since the batch of the beryllium used for the FM and QM models was identical, the calibration data for the beryllium spectral transmission were valid. The absolute thickness of the filter would then have been calibrated in flight. It was found that the only relevant contaminant in the beryllium foil was a small amount of iron (Fe). Figure 23 shows the tiny drop in filter transmission around the Fe-K edge.
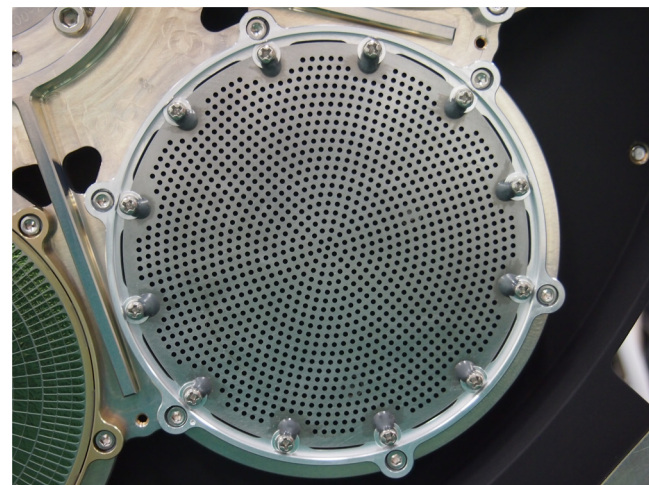

Fig. 24 Picture of the neutral density filter, mounted in the filter wheel disk. It consists of a molybdenum sheet with holes.

4.2 Neutral Density Filter

The second x-ray filter is the neutral density filter. This consists of a molybdenum sheet with holes (see Fig. 24). The sheet has a thickness of 0.25 mm, and the hole diameter is 1.1 mm. The total opening of all holes defines the transmission of the filter, which was computed at 24.5%. Molybdenum was selected as filter material because the major fluorescent lines of this material are outside of the SXS energy band. The cosmic particle background radiation could otherwise generate additional background lines when the neutral density filter would be in the beam. This filter was intended to be used for very bright sources, to limit the flux equally across the energy band, in order to prevent the energy resolution to degrade due to high flux.

5 Future Prospects and Conclusions

The SXS filter wheel was a versatile instrument, enabling both filtering of the input x-rays through a set of filters to prevent loss of energy resolution due to high flux, as well as providing overall gain calibration for all SXS pixels through a set of

calibration sources. Due to the limited operational life of the satellite, most of the filter-wheel functions were not used. However, the ^{55}Fe calibration sources were crucial for obtaining key data on the SXS pixel gain behavior, used for the scientific analysis of the Perseus cluster observations.[5] The active MXS calibration sources are a new type of x-ray sources to be used in space. Although not (yet) activated during the actual Hitomi mission, experience gained with these sources while developing and using them during Hitomi ground tests proved them to be very reliable. The advantage of such sources is that they can be tuned both in the time domain (up to short duration pulses of 1 ms and less) as well as their flux levels. Similar sources are now being considered for future missions, such as a Hitomi successor mission (currently referred to as XARM) and the XIFU instrument on the Athena spacecraft.[16]

Acknowledgments

References

1. R. L. Kelley et al., "The Astro-H high resolution soft x-ray spectrometer," *Proc. SPIE* **9905**, 99050V (2016).

2. T. Takahashi et al., "The ASTRO-H (Hitomi) x-ray astronomy satellite," *Proc. SPIE* **9905**, 99050U (2016).

3. M. Tsujimoto et al., "In-orbit operation of the ASTRO-H SXS," *Proc. SPIE* **9905**, 99050Y (2016).

4. C. A. Kilbourne et al., "The design, implementation, and performance of the Astro-H SXS calorimeter array and anti-coincidence detector," *Proc. SPIE* **9905**, 99053L (2016).

5. Hitomi Collaboration, "The quiescent intracluster medium in the core of the Perseus cluster," *Nature* **535**, 117–121 (2016).

6. C. A. Kilbourne et al., "The design, implementation, and performance of the Astro-H SXS aperture assembly and blocking filters," *Proc. SPIE* **9905**, 99053Q (2016).

7. P. J. Shirron et al., "Design and on-orbit operation of the adiabatic demagnetization refrigerator on the Hitomi soft x-ray spectrometer instrument," *Proc. SPIE* **9905**, 99053O (2016).

8. C. P. de Vries et al., "Filters and calibration sources for the soft x-ray spectrometer (SXS) instrument on ASTRO-H," *Proc. SPIE* **7732**, 773213 (2010).

9. C. P. de Vries et al., "Calibration sources for the soft x-ray spectrometer instrument on ASTRO-H," *Proc. SPIE* **8443**, 844353 (2012).

10. M. E. Eckart et al., "Ground calibration of the Astro-H (Hitomi) soft x-ray spectrometer," *Proc. SPIE* **9905**, 99053W (2016).

11. K. Gendreau, Private communication (2008).

12. K. Gendreau, "Miniaturized, high-speed, modulated x-ray source," 2013, https://ntrs.nasa.gov/search.jsp?R=20130014145 (16 October 2017).

13. M. E. Eckart, K. Kilbourne, and F. S. Porter, "Instrument calibration report natural line shapes of SXS onboard calibration sources," 2016, https://heasarc.gsfc.nasa.gov/docs/hitomi/calib/caldb_doc/asth_sxs_caldb_linefit_v20161223.pdf (16 October 2017).

14. T. Yaqoob, "Instrument calibration report SXS gate valve and filter wheel filters," 2016, https://heasarc.gsfc.nasa.gov/docs/hitomi/calib/caldb_doc/asth_sxs_caldb_filterfiles_v20161223.pdf (16 October 2017).

15. S. Takeda et al., "Performance verification and system integration tests of the pulse shape processor for the soft x-ray spectrometer onboard ASTRO-H," *Proc. SPIE* **9144**, 91445B (2014).

16. D. Barret et al., "The Athena x-ray integral field unit (X-IFU)," *Proc. SPIE* **9905**, 99052F (2016).

Biographies for the authors are not available.